

Power Distribution Control between Cells with Imbalanced Load for Modular Multilevel Multiport Converter

Takumi Yasuda
 Dept. of Science of Technology
 Innovation
 Nagaoka University of Technology
 Nagaoka, Japan
 t_yasuda@stn.nagaokaut.ac.jp

Jun-ichi Itoh
 Dept. of Science of Technology
 Innovation
 Nagaoka University of Technology
 Nagaoka, Japan
 itoh@vos.nagaokaut.ac.jp

Giuseppe Guidi
 Energy Systems
 SINTEF Energy Research
 Trondheim, Norway
 Giuseppe.Guidi@sintef.no

Abstract— This paper proposes a balancing control method for load imbalance in one arm of a multiport converter based on a modular multilevel converter (MMC) topology. In the multiport converter with load imbalance, a balanced three-phase current is achieved thanks to power distribution control. However, the multiport converter has a limitation on the amount of load imbalance that can be compensated. This paper derives the theoretical limitation of the compensation capabilities using the proposed balance control for the load imbalance. The proposed control method is demonstrated by simulation, showing that balanced three-phase grid current is obtained in spite of the load imbalance and that the DC link voltage error is limited to 1.4%. In addition, simulation and experimental results clarify that the proposed controller has larger compensation capability for the load imbalance compared to the conventional control strategy.

Keywords—multiport converter, modular multilevel converter, intra-arm balance controller

I. INTRODUCTION

In recent years, multiport converters have been actively researched along with the development of a smart-grid and renewable energy sources [1]-[2]. In particular, the multiport converter with an MMC topology has been proposed as a large-capacity battery energy storage system (BESS), a PV power conditioner, and so on [3]-[5].

Fig. 1 depicts a multiport converter based on MMC for BESS. The loads modeling the battery modules are connected to each cell. The cascaded structure with low-voltage devices eliminates the necessity of the line frequency transformer to connect to the medium voltage grid and reduces the system volume and the cost. In addition, the MMC topology has a better fault-tolerance than other converter topologies thanks to its high flexibility and scalability.

In the multiport converter, the power is interchanged among cells in order to achieve both the balanced grid current and the desired power distribution. Intra-arm balance controller injects a different compensation voltage to the input voltage of the cell in order to compensates the load imbalance among the cell belonging to the same arm. However, the intra-arm balance controller has a limitation of the compensation capability due to the over-modulation. Many studies have utilized the conventional intra-arm balancing controller, which distributes the arm voltage reference to the cell in proportion to the load of the cell [5]-[7]. In contrast, the intra-arm balance controller in [8] has improved the compensation

capability by an optimized combination of DC and the grid frequency component of the input voltage of the cell. However, the method in [8] does not consider the optimized phase angle of the grid frequency component. In contrast, Ref. [9] adjusts the phase angle of the input voltage of the cell to extend the compensation capability for the multi-port converter based on MMC with single-star bridge cells (MMC-SSBC). However, the DC component is not considered in [9] because MMC-SSBC has no capability of flowing the DC current due to its topology. Therefore, the intra-arm balancing controller in [9] is not suitable for the multiport converter shown in Fig. 1.

This paper proposes an intra-arm balance controller with an extended compensation capability. The proposed controller changes the frequency of compensation voltage depending on the state of the arm current. In addition, the theoretical limit of the load imbalance that can be compensated with the proposed controller is clarified. The proposed method is evaluated by simulations and experiments. The simulation and the experimental result under the load imbalance of 8.0% demonstrates that the total harmonic distortion (THD) of the three-phase grid current becomes 0.9% and DC link voltage error is limited to 1.4% thanks to the proposed method. Furthermore, these results show that the selection of the compensation voltage has little effect on the other controllers.

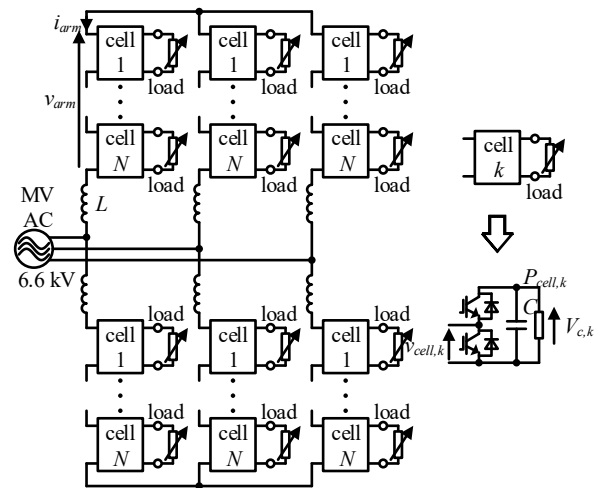


Fig. 1. Concept of multiport converter based on MMC.

II. CONTROL STRATEGY FOR MULTI-PORT CONVERTER

This paper discusses the operation of the system when different loads are connected to each cell. The cells interchange the power with each other in order to balance the grid current.

A. Overview of controllers for multiport converter

Fig. 2 illustrates an outline of the control block diagram for the multiport converter. The grid side control part and the balance control part in Fig. 2 are the same to the control method of the conventional MMC [4]. The traditional PI control is applied for each controller in this paper. The grid side control part is implemented for the balanced three-phase grid current. The total power controller controls input power to the converter. The balance controller compensates the load imbalance between the arms by the circulating current. The circulating current consists of the DC and the grid frequency component. The sum of the outputs from the grid side control part and the balance control part is the command of the arm voltage v_{arm}^* , which consists of the DC and the grid frequency component as in,

$$v_{arm} = \frac{NV_c}{2} + \sqrt{2}V_g \cos \omega_g t, \quad (1)$$

where N is the number of cells in one arm, V_c is the DC link voltage of the cell, V_g is the RMS value of the grid phase voltage, and ω_g is the angular frequency of the grid. The DC link voltage V_c is assumed to contain no ripple voltage in the following theoretical analysis. The arm current is the sum of the grid current $i_g/2$, which is distributed to the upper and lower arms evenly, the DC current I_0 used for power interchange between the phases, and the grid frequency component i_ω used for power interchange between the upper and the lower arms, as shown in,

$$i_{arm} = \frac{1}{2}i_g + I_0 + i_\omega \equiv I_0 + \sqrt{2}I_1 \cos(\omega_g t + \phi_i), \quad (2)$$

where ϕ_i is the phase difference of the arm current from the grid frequency component of the arm voltage v_{arm} .

Voltage redundancy ρ is defined for the following analysis as,

$$\rho = \frac{NV_c}{2\sqrt{2}V_g}. \quad (3)$$

The voltage redundancy ρ indicates the ratio of the peak-peak value of the arm voltage in (1) and the maximum output voltage of one arm. The voltage redundancy of more than 1 is necessary to shape the arm voltage without zero sequence voltage, which is the condition for this paper.

B. Proposed intra-arm balance control

Fig. 3 depicts the proposed intra-arm balance controller. The intra-arm balance controller regulates the DC link voltage of the cells in one arm with the DC or the grid frequency compensation voltage. Larger amplitude of the compensation voltage is required as the load imbalance increases. Meanwhile, the injection of the large compensation voltage may cause the over-modulation. The proposed intra-arm balance controller has two operation modes and selects the mode which compensates the load imbalance with a smaller amplitude of the input voltage of the cell. The proposed controller contains the following two compensation

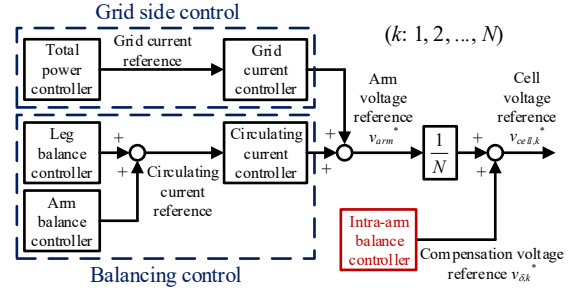


Fig. 2. Control block diagram.

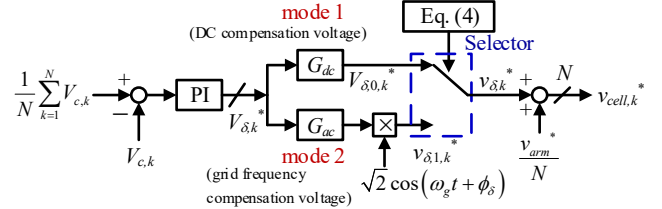


Fig. 3. Proposed intra-arm balance controller.

methods.

<mode 1> DC voltage compensation mode: DC voltage is utilized for the compensation voltage $v_{\delta,k}$.

<mode 2> Grid frequency voltage compensation mode: Grid frequency component is utilized for the compensation voltage $v_{\delta,k}$. In the grid frequency voltage compensation mode, the phase angle of the compensation voltage ϕ_δ is set according to the phase angle of the arm current ϕ_i to achieve a maximized compensation capability.

The compensation capabilities of mode 1 and mode 2 depend on the arm current. For instance, under the arm current condition of $I_0 = 0$, the load imbalance cannot be compensated with mode 1 because the DC voltage generates no active power. Similarly, mode 2 has no compensation capability under the condition of $I_1 = 0$. Thus, the mode selection is performed according to the arm current. Mode 1 is selected under the arm current condition expressed in (4).

$$\sqrt{2}(\rho - 1)|I_0| \geq \left(\rho - \max \left[\frac{1}{\rho}, |\cos \phi_i| \right] \right) I_1. \quad (4)$$

The proposed controller selects mode 2 when (4) is false. The proposed control extends the compensation capability by selection of the modes with (4) compared to the conventional controllers. The sum of the compensation voltage injected to each cell in one arm is always zero and the arm voltage v_{arm} always follows (1) in any loaded condition. Hence, the intra-arm balance controller does not affect the other controllers even when the mode change.

The compensation power becomes maximum when the input voltage of the cell becomes in-phase with the arm current as a result of injection of the compensation voltage. On the other hand, the compensation power becomes minimum when the phase angle of the input voltage of the cell becomes opposite to the phase angle of the arm current. However, the maximum and the minimum compensation power cannot be achieved with same phase angle of the reference waveform ϕ_δ . In order to improve the compensation capability, the phase angle of the compensation voltage is set as,

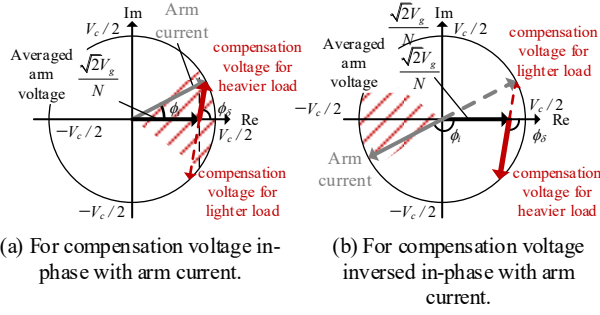


Fig. 4. Phasor diagram of grid frequency component of reference waveform $\sin(\omega_g t + \phi_s)$.

$$\phi_s = \begin{cases} \tan^{-1} \frac{\rho \sin \phi_i}{\rho \cos \phi_i - 1} & \dots \left(\cos \phi_i > \frac{1}{\rho} \right) \\ \pi - \tan^{-1} \frac{\rho \sin \phi_i}{\rho \cos \phi_i + 1} & \dots \left(\cos \phi_i < -\frac{1}{\rho} \right) \\ \text{sign}[\phi_i] \cdot \frac{\pi}{2} & \dots \left(|\cos \phi_i| \geq \frac{1}{\rho} \right) \end{cases}. \quad (5)$$

Fig. 4 shows phasor diagrams of the compensation voltage of the grid voltage compensation mode (mode 2). In mode 2, the phase angle of the reference waveform ϕ_s is set according to the arm current. The maximum available amplitude of the grid frequency component of the input voltage for the cell is $V_c/2$. The compensation voltage is injected to the averaged arm voltage v_{arm}^*/N as in Fig. 4. Fig. 4(a) shows the first row of (5). This condition is enabled when the phase angle of the arm current ϕ_i is close to that of the arm voltage. As a result of the injection of the compensation voltage, the input voltage of the cell can be in-phase with the arm current ϕ . Hence, the compensation capability for the heavier load is maximized. In this condition, the compensation capability for the lighter load imbalance is larger than that for the heavier load imbalance. That is because the large amplitude of the compensation voltage is available for the compensation of the lighter load imbalance as shown in Fig. 4(a). Fig. 4(b) shows the second row of (5). This condition is enabled when the phase difference of the arm current and the arm voltage is relatively large. The phase angle of the input voltage for the cell can be inverted with respect to the arm current by the compensation voltage. Hence, the compensation capability for the lighter load imbalance is maximized. In this condition, the compensation capability for the heavier load imbalance is larger than that for the lighter load imbalance. That is because the larger amplitude of the compensation voltage is available for the compensation of the heavier load imbalance. Fig. 4(c) shows the third row of (5). This condition is enabled when the imaginary part of the arm current is relatively large as in Fig. 4(c). In this condition, the proposed controller has same compensation capabilities for the heavier and the lighter load

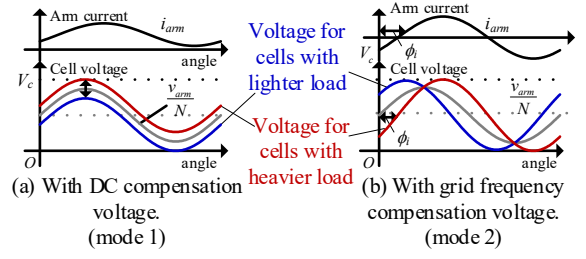


Fig. 5. Example of cell voltages with proposed intra-arm balance control under imbalanced load in one arm.

imbalance.

Fig. 5 illustrates an example of the input voltages for the cell with the proposed method. In mode 1 shown in Fig. 5(a), the proposed controller injects the DC voltage to the input voltage for the cell in order to compensate the load imbalance. On the other hand, the proposed controller in mode 2 injects the grid frequency voltage as shown in Fig. 5(b). In mode 2, the phase difference between the arm current and the input voltage for the cells is decreased as the cell has the heavier load imbalance. Meanwhile, the phase difference is increased as the cell has the lighter load imbalance. The input power to each cell tracks to the command thanks to the proposed controller.

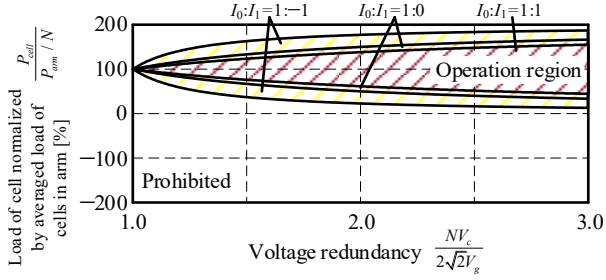
III. THEORETICAL COMPENSATION CAPABILITY OF PROPOSED INTRA-ARM BALANCE CONTROLLER

The command of the input voltage for the cell is decided by the loads of the cells in the converter. In order to prevent the over-modulation, there is a limitation of the compensation capability for the load imbalance with the proposed controller. The minimum value of the input voltage for cell has to be larger than zero and the maximum value of the of the input voltage for cell has to be smaller than the DC link voltage of cell V_c as in,

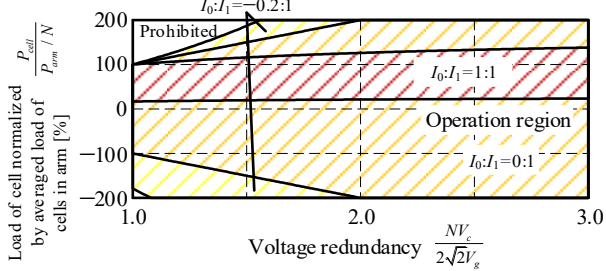
$$0 \leq v_{cell,k}(t) \leq V_c. \quad (6)$$

Equation (6) causes the limitation of the compensation capabilities due to the limitation of the available amplitude of the compensation voltage.

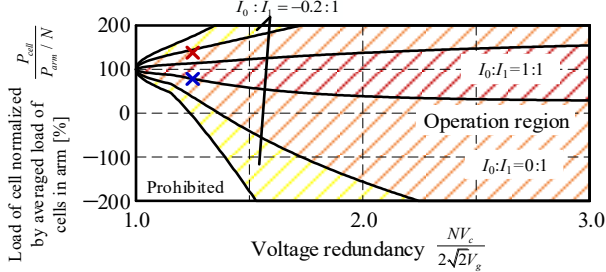
Fig. 6 presents the limitation of the compensation capability of the proposed intra-arm balance controller derived from (6). Voltage redundancy ρ is shown on the horizontal axis, and the load of each cell $P_{cell,k}$ normalized by the averaged load of the cells in the arm P_{arm}^*/N is shown on the vertical axis. The proposed controller is able to compensate the load imbalance when all loads in the arm are within the shaded region in Fig. 6. Otherwise, the arm current distortion occurs due to the over-modulation. The simulation and the experimental condition is indicated in Fig. 6(c). The larger voltage redundancy extends the operation region in both mode 1 and mode 2 because the larger voltage redundancy, which means larger DC link voltage V_c , increases the maximum available amplitude of the compensation voltage. In mode 1, the operation region extends as the DC current I_0 increases compared to the grid frequency component I_1 as shown in Fig. 6(a). In the grid frequency voltage compensation mode, the operation region extends as the grid frequency component of arm current I_1 increases compared to the DC current I_0 as shown in Fig. 6(b). In addition, the operation region with the heavier load imbalance extends when the phase difference of the arm current ϕ_i^* increases as in Fig. 6(b) and (c). On the other hand, the operation region with the lighter load



(a) With DC compensation voltage. (mode 1)



(b) With grid frequency compensation voltage (mode 2) and $\phi_i^* = 0$.



(c) With grid frequency compensation voltage (mode 2) and $\phi_i^* = \pi/6$. The maximum and the minimum load imbalance for the following simulation and experimental conditions (Fig. 8 and Fig. 12) are indicated.

Fig. 6. Theoretical maximum/minimum input power to cell.

imbalance becomes narrower when the phase angle of the arm current ϕ_i^* increases.

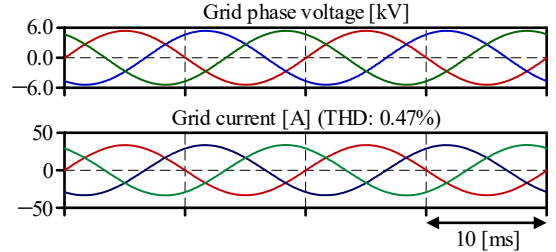
IV. SIMULATION RESULT

Table I describes the simulation conditions. The maximum load imbalance between the cells in each arm is 8.0% and they satisfy the limitation as shown in (6). The unit capacitance constant (UCC) [10] of the cell capacitor is set to 35 mJ/VA.

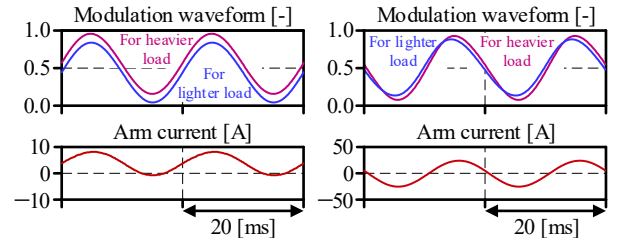
Fig. 7 shows the steady state operation of the multiport converter with the proposed controller. Fig. 7(a) shows the grid phase voltage and current. The grid current with the proposed method is balanced with a THD of 0.40% and unity power factor. Fig. 7(b) shows the modulation waveforms for the cell with mode 1. The modulation waveforms for the cell with the heavier load has the larger DC component than that for the cells with the lighter load in order to compensate the load imbalance. Fig. 7(c) shows the modulation waveforms with mode 2. The modulation waveforms for the cell with the heavier load has larger amplitude of the grid frequency component for the compensation of the load imbalance. In addition, the phase angle of the modulation waveform for the cell with the heavier load becomes close to the phase angle of the arm current. The proposed controller selects the compensation voltage according to the state of the arm current. Fig. 7(d) shows the DC link voltage of all 300 cells. The voltage error between the averaged DC link voltage of each cell and the command value of 246 V is approximately 1.6 V,

TABLE I. SIMULATION CONDITIONS.

Parameter	Symbol	Value
Rated power of cell	P_{cell}	2.2 kW
Grid line-line voltage	$\sqrt{3}V_g$	6.6 kV (RMS)
Grid frequency	f_g	50 Hz
Number of cells per arm	N	50
DC link voltage of cell	V_c	269 V
Arm inductance	L	70 mH (0.20p.u.)
Cell capacitance	C	2.1 mF (UCC=35 mJ/VA)

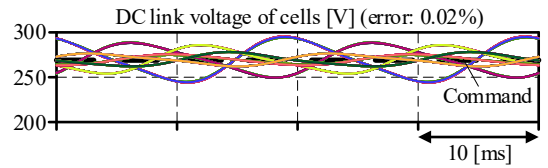


(a) Grid phase voltage and grid current.



(b) Modulation waveforms for cells with DC compensation voltage (mode 1).

(c) Modulation waveforms for cells with grid frequency compensation voltage (mode 2).



(d) DC link voltage of all 300 cells.

Fig. 7. Simulation result of steady state operation with the proposed method.

which is approximately 0.5%. These simulation results verify the validity of the proposed controller.

Fig. 8 shows the operation when the intra-arm balancing controller is switched from the proposed controller to the conventional controller [5]-[7]. The loaded condition is indicated in Fig. 6(c). The loaded condition satisfies (6) when the proposed controller is applied, whereas it does not satisfy (6) when the conventional controller is applied. The converter gains of these controllers are adjusted so as to prevent a shock at the controller change. Before the change, the cells operate without over-modulation and the DC link voltage of the cells are balanced. After the controller changes, the modulation waveforms for some cells begin to saturate because the conventional controller cannot compensate the load imbalance without the over-modulation. The DC link voltages of cells are converged even if the conventional controller is applied. However, the over-modulation caused by the conventional controller results in the distortion of the grid current as shown in comparison with Fig. 8(b)-(c). This simulation result reveals that the proposed controller compensates larger load imbalance than the conventional controller.

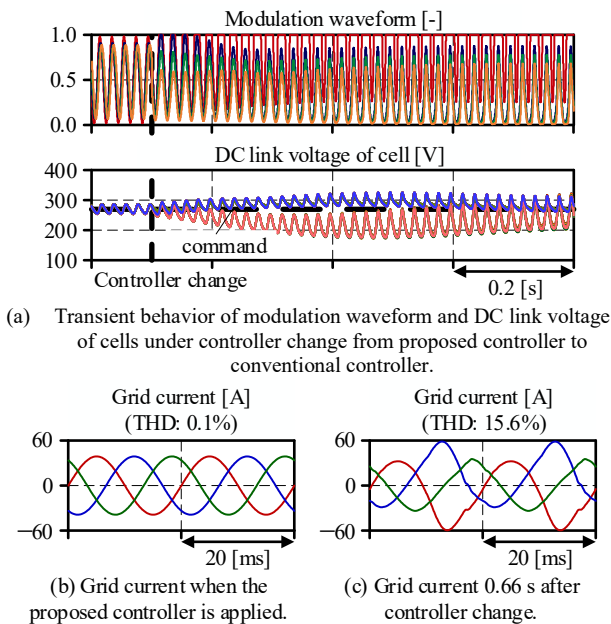


Fig. 8. Simulation result of operation with proposed controller and conventional controller.

V. EXPERIMENTAL RESULT

Fig. 9 shows the experimental setups. Table II describes the experimental condition. The parameters for the simulation are scaled down. The load imbalance in one arm of 8.0% is added as in the simulated condition.

Fig. 10 depicts experimental waveforms of the steady state operation of the multiport converter. Fig. 10(a) shows the experimental result of the grid current with the proposed controller. The grid current is balanced and in-phase with the grid phase voltage. THD of the grid current is 0.9%. Fig. 10(b) and (c) show the modulation waveforms for the cells with mode 1 and mode 2, respectively. The proposed controller selects the compensation voltage according to the state of the arm current as the simulation results. Fig. 10(d) shows the DC link voltage of the cells in the phase. The voltage error between the averaged DC link voltage of each cell and the command value of 21 V is 0.29 V, which is approximately 0.14%. These experimental results also verify the validity of the proposed controller.

Fig. 11 shows the transient behavior under a load change that causes a change in the compensation mode. The load is balanced before the load change and the load imbalance after the load change are in the theoretical compensation capability of the proposed controller as indicated in Fig. 6(c). After the load change, a DC link voltage error appears and the DC compensation voltage is injected to the modulation waveform because the arm current has relatively large DC component before the load change. The grid frequency component of the arm current is increased in order to compensate the load imbalance between arms caused by the load change. As a result, the proposed controller switches the mode and changes the compensation voltage from the DC component to the grid frequency component 0.14 s after the load change. The mode switching of the proposed controller does not affect neither the grid current nor the DC link voltage. The DC link voltage converges to the command value of 21 V within 0.2 s after the load change. This experimental result clarifies that the proposed controller compensates the load imbalance without



Fig. 9. The experimental setup of multiport converter prototype.

TABLE II. SIMULATION CONDITIONS.

Parameter	Symbol	Value
Rated power of cell	P_{cell}	90 W
Grid line-line voltage	$\sqrt{3}V_g$	122 V (RMS)
Grid frequency	f_g	50 Hz
Number of cells per arm	N	12
DC link voltage of cell	V_c	21 V
Arm inductance	L	1.5 mH (0.20p.u.)
Cell capacitance	C	15 mF (UCC=35 mJ/VA)

any effect on the other control loops, even in the event of a mode change.

Fig. 12 shows waveforms when the intra-arm balancing controller is changed from the proposed controller to the conventional controller [5]-[7]. The loaded conditions and the converter gain are set same as in the simulation of Fig. 8. Before the controller change, the cells operate without over-modulation and both the grid current and the DC link voltage of the cells are balanced. After the controller changes, the modulation waveforms for some cells are saturated. The conventional intra-arm balancing controller cannot compensate the load imbalance without entering over-modulation. The DC link voltages of the cells are balanced by the conventional controller. However, the over-modulation caused by the conventional controller increases the DC current to the grid as shown in comparison with Fig. 12(b)-(c). This experimental result verifies the theoretical analysis and the extended compensation capability of the proposed controller compared with the conventional method.

VI. CONCLUSIONS

This paper proposed an intra-arm balance controller with an extended compensation capability. The proposed controller changes the frequency of compensation voltage with larger compensation capability depending on the state of the arm current. In addition, the limitation of the proposed controller was clarified for the load imbalance conditions. The proposed method was evaluated by simulations and experiments. The simulation and the experimental result with the load imbalance of 8.0% demonstrated that THD of three-phase current became 0.9% and DC link voltage error became less than 1.4% thanks to the proposed method. Furthermore, these

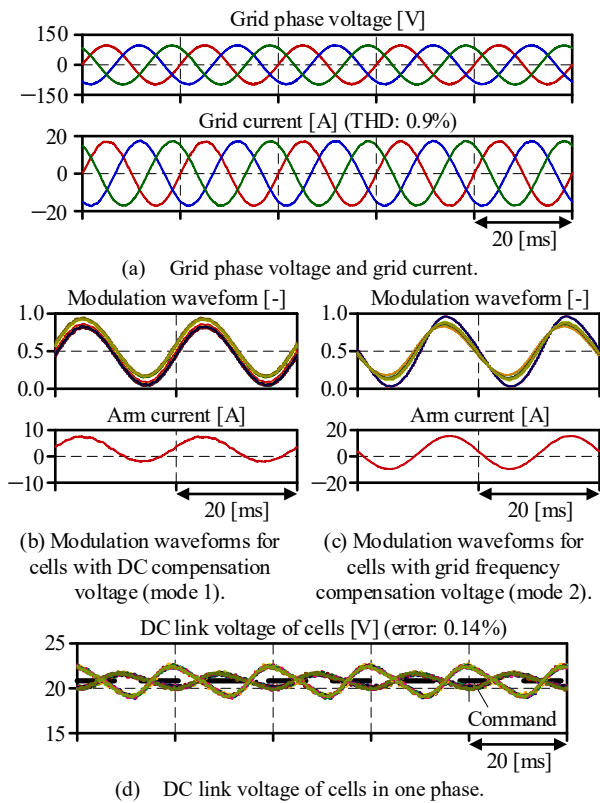


Fig. 10. Experimental result of steady state operation with the proposed method.

results showed that the selection of the compensation voltage had little effect on the other controllers in the system.

ACKNOWLEDGMENT

This work was supported by the project Modular Megawatt range Wireless EV Charging Infrastructure Providing Smart Grid Services (MoMeWeC), funded under the EIG CONCERT Japan program, Joint Call on Efficient Energy Storage and Distribution, with project number 284231.

REFERENCES

- [1] O. M. Toledo, D. O. Filho, A. S. A. C. Diniz, "Distributed Photovoltaic Generation and Energy Storage Systems: A Review," in *Renewable and Sustainable Energy Reviews*, vol. 14, no. 1, pp. 506-511, Jan. 2010.
- [2] Z. Rehman, I. Al-Bahadly, and S. Mukhopadhyay, "Multiinput DC-DC converters in renewable energy applications – An overview," in *Renewable and Sustainable Energy Review*, vol. 41, pp. 521-539, Jan. 2015.
- [3] G. Wang et al., "A Review of Power Electronics for Grid Connection of Utility-Scale Battery Energy Storage Systems," in *IEEE Transactions on Sustainable Energy*, vol. 7, no. 4, pp. 1778-1790, Oct. 2016.
- [4] G. Guidi, S. D'Arco, K. Nishikawa and J. A. Suul, "Load Balancing of a Modular Multilevel Grid Interface Converter for Transformer-Less Large-Scale Wireless Electric Vehicle Charging Infrastructure," in *IEEE Journal of Emerging and Selected Topics in Power Electronics*.
- [5] P. Sochor and H. Akagi, "Theoretical and Experimental Comparison Between Phase-Shifted PWM and Level-Shifted PWM in a Modular Multilevel SDBC Inverter for Utility-Scale Photovoltaic Applications," in *IEEE Transactions on Industry Applications*, vol. 53, no. 5, pp. 4695-4707, Sept.-Oct. 2017.
- [6] L. Maharjan, T. Yamagishi and H. Akagi, "Active-Power Control of Individual Converter Cells for a Battery Energy Storage System Based

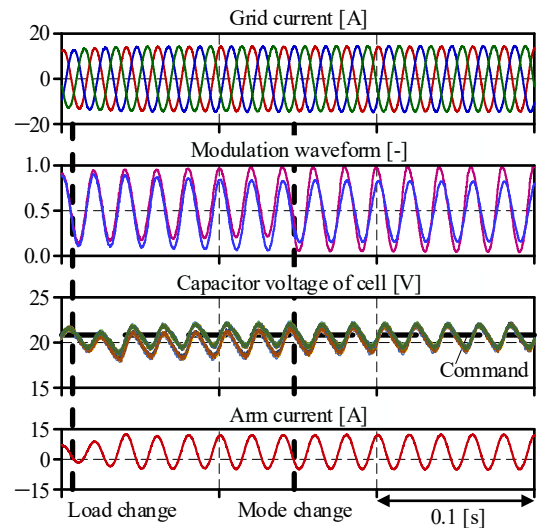
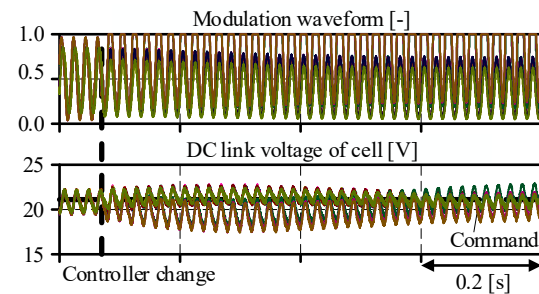
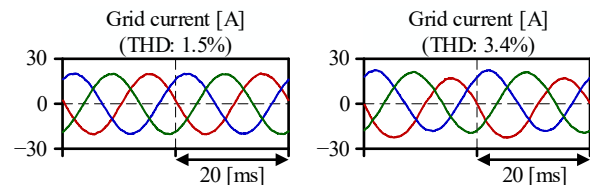


Fig. 11. Experimental result of transient behavior with proposed method under load change.



(a) Transient behavior of modulation waveform and DC link voltage of cells under converter change from proposed controller to conventional controller.



(b) Grid current when the proposed controller is applied. (c) Grid current 0.36 s after the controller change.

Fig. 12. Experimental result of transient behavior under controller change from proposed controller to conventional controller.

on a Multilevel Cascade PWM Converter," in *IEEE Transactions on Power Electronics*, vol. 27, no. 3, pp. 1099-1107, March 2012.

- [7] T. Zhao et al., "Harmonic Compensation Strategy for Extending the Operating Range of Cascaded H-Bridge PV Inverter," in *IEEE Journal of Emerging and Selected Topics in Power Electronics*, vol. 8, no. 2, pp. 1341-1350, June 2020.
- [8] Z. Wang, H. Lin, and Y. Ma, "Improved Capacitor Voltage Balancing Control for Multimode Operation of Modular Multilevel Converter with Integrated Battery Energy Storage System," in *IET Power Electronics*, vol. 12, no. 1, pp. 2751-2760, Spet. 2019.
- [9] L. Liu, H. Li, Y. Xue and W. Liu, "Reactive Power Compensation and Optimization Strategy for Grid-Interactive Cascaded Photovoltaic Systems," in *IEEE Transactions on Power Electronics*, vol. 30, no. 1, pp. 188-202, Jan. 2015.
- [10] H. Fujita, S. Tominaga, and H. Akagi, "Analysis and design of a DC voltage-controlled static VAR compensator using quad-series voltagesource inverters," in *IEEE Transactions on Industry Applications*, vol. 32, no. 4, pp. 970-978, July-Aug. 1996.